Horizontal Deformation Rate Analysis Based on Multiepoch GPS Measurements in Shanghai

Jianqing Cai[1]; Jiexian Wang[2]; Jicang Wu[3]; Congwei Hu[4]; Erik Grafarend[5]; and Junping Chen[6]

Abstract: By applying integrated least-squares adjustment of multicampaigns geographic positioning system (GPS) measurements, the velocity of any GPS monument can be obtained. The resulting velocities are used to estimate the strain rate tensors and their variances under infinitesimal strain assumption in a discrete triangle. In this paper, the GPS measurements of five campaigns, which were carried out in Shanghai City from 2002 to 2005, are used to determine the velocity of each GPS monument. Then the horizontal strain rate tensors are calculated with the relative velocities of the sites obtained. The analysis of these principal strain rates together with a comparison of the geological information is performed. The patterns of the principal strain rates show a significant northwest to southeast extension zone in the southwestern part of Shanghai, which agrees well with the neo-tectonic activity of an existing geological fault, the so-called "Dachang–Zhoupu" fault.

DOI: 10.1061/(ASCE)0733-9453(2008)134:4(132)

CE Database subject headings: Strain rate; Geodetic surveys; Velocity; Data processing; Deformation.

Introduction

With high-precision geodetic global positioning system (GPS) receivers as well as strict surveying procedures and data processing methods, the continuous or campaign GPS surveying can be used to detect ground deformation with an horizontal accuracy of 0.1 cm/year and a vertical accuracy of 0.3 cm/year (Shen et al. 2000; Wang et al. 2001). GPS observations have been widely used for monitoring crustal deformation, landslide, and ground subsidence (Sagiya et al. 2000; Kim et al. 2003; Leick 2004; Kaniuth and Vetter 2005; Wu et al. 2006). Shanghai is one of the biggest cities in China. It is located on the coast of the East China Sea. Its average elevation is only about 4 m. With the fast economic development, the local government is paying greater attention to the ground deformation which is a result of active faults and city subsidence caused by the extraction of underground water and the constructions of more skyscrapers. A GPS network with more than 20 points including four continuous sites has been set up which enabled the Institute of Shanghai Geological Surveying (ISGS) to carry out campaign GPS surveying every year starting from 2002 to monitor horizontal ground deformation and subsidence.

In the deformation analysis in geosciences (geodesy, geophysics, and geology), we are often confronted with the problem of a two-dimensional (2D) (or planar and horizontal), symmetric rank-two deformation tensor. Its eigenspace components (principal components, principal direction) play an important role in interpreting phenomena like earthquakes (seismic deformations), plate motions, and plate deformations, among others. In our recent papers on statistical analysis of random deformation tensor (Cai 2004; Cai et al. 2005) we have achieved the complete solution to the statistical inference of *eigenspace components* of a 2D random tensor, which includes the best linear uniformly unbiased estimation (BLUUE) of the eigenspace elements and the best invariant quadratic uniformly unbiased estimate (BIQUUE) of its variance–covariance matrix together with the design of a linear hypothesis test. This solution proposes a multivariate model to statistically process random tensors in the eigenspace and, in particular, applies the technique to analyze the repeated geodetic measurements. Unlike most geophysical applications of the same kind, this solution focuses on the statistical inference of the significance of the computed random tensors to support their interpretations. With these models we have successfully performed the statistical inference of the *eigenspace components* vector and the variance-covariance matrix of the *Gauss–Laplace* normally distributed observations of a random deformation tensor derived from the ITRF data sets in the central Mediterranean, Western Europe, and Fennoscandia (Cai and Grafarend 2007a,b; Cai et al. 2008).

In this study, all campaign GPS data are processed by GAMIT software (King and Bock 2005) as a daily solution and corresponding baseline vectors are obtained. Then, an integrated adjustment method is implemented to estimate all baseline vectors

[1]Dr.-Ing., Institute of Geodesy, Global Positioning System (GPS), Stuttgart Univ., Geschwister-Scholl-Str. 24D, 70174 Stuttgart, Germany (corresponding author). E-mail: cai@gis.uni-stuttgart.de

[2]Professor, Dept. of Surveying and Geo-Informatics, Tongji Univ., 1239 Siping Rd., Shanghai 200092, P. R. China. E-mail: wangjiexian@mail.tongji.edu.cn

[3]Professor, Dept. of Surveying and Geo-Informatics, Tongji Univ., 1239 Siping Rd., Shanghai 200092, P. R. China. E-mail: jcwu@mail.tongji.edu.cn

[4]Associate Professor, Dept. of Surveying and Geo-Informatics, Tongji Univ., 1239 Siping Rd., Shanghai 200092, P. R. China. E-mail: cwhu@mail.tongji.edu.cn

[5]Professor, Institute of Geodesy, Stuttgart Univ., Geschwister-Scholl-Str. 24D, 70174 Stuttgart, Germany. E-mail: erik.grafarend@gis.uni-stuttgart.de

[6]Doctor, GeoForschungsZentrum Potsdam, Telegrafenberg A17,14473 Potsdam, Germany. E-mail: junping.chen@gfz-potsdam.de

Note. Discussion open until April 1, 2009. Separate discussions must be submitted for individual papers. The manuscript for this paper was submitted for review and possible publication on June 21, 2007; approved on January 15, 2008. This paper is part of the ***Journal of Surveying Engineering***, Vol. 134, No. 4, November 1, 2008. ©ASCE, ISSN 0733-9453/2008/4-132–137/$25.00.

Table 1. Details of Each GPS Surveying Campaign

Campaign	Mean time Year)	Mean time (Day)	Duration[a] (days)	Session (h)	Logging rate (s)	Number of sites	Instrument
1	2002	252	7	24	30	26	6 sets, Ashtech Z12
2	2003	038	7	24	30	28	6 sets, Ashtech Z12
3	2003	216	7	24	30	36	6 sets, Ashtech Z12
4	2004	162	33	24	30	65	10 sets, Ashtech Z12
5	2005	179	15	24	30	90	14 sets, Ashtech Z12

[a]Since fourth campaign, four continuous GPS sites have been in operation.

together. The relative velocities of 17 common sites are determined together with their standard deviations. After that, the strain rate tensors are calculated and the relative velocities obtained, and the principal components of horizontal strain rate tensors together with their variance-covariance matrices are determined in each discrete triangle. With the presentation of the pattern of these principal strain rates, an analysis and a comparison with the geological information are performed. Finally, some conclusions are given.

GPS Surveying and Relative Velocities

Between September 2002 and May 2005, five GPS surveying campaigns were conducted by ISGS in Shanghai. Table 1 shows detailed information for each campaign, including mean time of the epoch, total number of measured GPS sites, session time, duration of the campaign, and GPS receiver information. As the city area of Shanghai is developing rapidly, the locations of some GPS sites have been changed due to construction work or environmental changes. There are only 17 GPS sites which could be observed in common during all five campaigns. On the other hand, more GPS monitoring sites have been set up in recent years to receive a higher density of observations or to cover more area.

GPS data processing strategy is based on a daily solution, which contains all independent baseline vectors and a covariance matrix. GAMIT software is used in this step international GPS services final orbit and earth rotational parameters are fixed. The ITRF2000 reference station, SHAO, in Shanghai is fixed as the reference station. Afterwards, an integrated adjustment based on all the daily solutions is performed to derive station velocities. When conducting an integrated adjustment, all the baseline vectors should be reduced to the same coordinate frame and common time epoch (Soler 2001). In this paper, the ITRF2000 is used and the adjustment time epoch is set to the mean time of the five surveying campaigns. Thus, the coordinates of each station will equal the coordinates at the chosen adjustment epoch plus the product of velocity and duration interval, i.e.

$$\boldsymbol{\varepsilon}_k + \Delta\mathbf{R}_{ij} = \mathbf{R}_{jm} + \mathbf{V}_{XYZj} \cdot dt - \mathbf{R}_{im} - \mathbf{V}_{XYZi} \cdot dt \tag{1}$$

where $\Delta\mathbf{R}_{ij}=(\Delta X_{ij}\ \Delta Y_{ij}\ \Delta Z_{ij})^T$=baseline vector observed at epoch t from station i to station j with the corresponding residuals $\boldsymbol{\varepsilon}_k$ of the baseline vector. The vectors $\mathbf{R}_{jm}$ and $\mathbf{R}_{im}$ contain the coordinates of stations i and j at epoch t_m which is the mean time of the first epoch t_f and the last epoch t_l; in other words $t_m=(t_l+t_f)/2$, dt is defined as

$$dt = \frac{t - t_m}{\delta}, \quad \delta = \frac{t_l - t_f}{2} \tag{2}$$

$\mathbf{V}_{XYZi}$ represents the three-dimensional velocity vector, the unit of $\mathbf{V}_{XYZi}$ is in m/δ. The domain of dt is $[-1,+1]$. In this case, the coordinate and velocity entries of the normal matrix will have the same order of magnitude. Thus, the least-squares estimation (LSE) based integrated adjustment will be more stable. In the integrated adjustment, the coordinate and velocity of SHAO are fixed at the chosen adjustment epoch. As a result, the coordinates of the other 16 GPS sites as well as their relative velocities with respect to the SHAO are obtained and listed in Table 2.

In Table 2, V_e and V_n=east and north components of the relative velocity, whereas σ_{Ve} and σ_{Vn}=corresponding standard deviations. The relative velocities range from about 0.1 to about 1 cm/year. Since the ground movement is not regular, the strain rate analysis using these velocities is conducted in the next section.

Strain Rates

Computation of Geodetic Strain Rate Tensor

The main objective of this study is to analyze the eigenspace component parameters of the two-dimensional strain rate tensor, which can be derived from the two-dimensional horizontal relative velocities of the 17 GPS sites in Shanghai with the methods introduced as follows.

When we select geodetic sites as vertices of convex polygons we can evaluate the strain tensor of the polygon by using the horizontal velocities. Let $[V_{E_i}\ V_{N_i}]'$ be the known horizontal residual velocity vector of the polygon vertex i along the east and north directions on the local geodetic coordinate system; the following approximation can be written (Devoti et al. 2002):

$$\begin{bmatrix} V_{E_i} \\ V_{N_i} \end{bmatrix} = \begin{bmatrix} V_{E_B} \\ V_{N_B} \end{bmatrix} + \begin{bmatrix} \frac{\partial V_E}{\partial E} & \frac{\partial V_E}{\partial N} \\ \frac{\partial V_N}{\partial E} & \frac{\partial V_N}{\partial N} \end{bmatrix} \begin{bmatrix} \Delta E_i \\ \Delta N_i \end{bmatrix} \Leftrightarrow \mathbf{V}_{EN_i} = \mathbf{V}_{EN_B} + \mathbf{L}\Delta\mathbf{X}_{EN} \tag{3}$$

where $[V_{E_B}V_{N_B}]'$=unknown velocity vector for a reference internal point B, $\mathbf{L}$=velocity gradient tensor, and $[\Delta E_i\ \Delta N_i]'$=coordinate difference between the site i and the reference point B, computed, respectively, as parallel and meridian arc lengths. According to Malvern (1969), $D=(L+L^T)/2$ is defined as deformation rate; and $R=(L-L^T)/2$ is defined as spin tensor, both evaluated at a point (E,N). Therefore, Eq. (3) gives an approximate method for calculating deformation rates D and R. In our research, the displacement and displacement gradient are considered to be very small, the infinitesimal strain rate tensor is approximately equal to the deformation rate, and the differential rotation rate tensors are approximately equal to the spin tensor (Malvern (1969); Dermanis and Livieratos 1983).

The approximation assumes a linear variation of the velocity components with respect to their coordinate differences. This

Table 2. Coordinates and Relative Velocities of 17 Common GPS Sites

Name	Latitude (DMS)[a]	Longitude (DMS)[a]	V_e (cm/year)	σ_{Ve} (cm/year)	V_n (cm/year)	σ_{Vn} (cm/year)
BC17	31-11-19	121-33-59	0.44	0.05	0.21	0.00
BS09	31-25-04	121.2750	−0.31	0.06	0.24	0.06
GL15	31-17-29	121-39-23	−0.25	0.05	0.17	0.00
HC21	31-13-27	121-19-19	−0.75	0.06	0.30	0.00
HT08	31-28-33	121-16-40	−0.44	0.08	0.64	0.08
TP20	31-17-04	121-22-36	−0.22	0.05	0.25	0.00
XZ02	31-10-52	121-25-16	0.00	0.00	0.00	0.00
CD29	31-00-08	121-18-03	−0.90	0.06	0.35	0.06
XH23	31-12-17	121-07-04	−0.16	0.05	−0.03	0.05
JC34	31-09-57	121-47-11	−0.19	0.04	0.30	0.04
SD28	31-00-48	121-44-48	−0.37	0.05	0.21	0.05
CX10	31-23-18	121-41-07	−0.18	0.04	0.19	0.04
HS14	31-20-32	121-50-15	−0.14	0.05	0.14	0.04
BZ37	31-33-42	121-38-00	−0.22	0.06	0.02	0.05
CJ07	31-30-14	121-47-55	−0.32	0.06	0.25	0.06
CM05	31-38-04	121-24-01	−0.34	0.11	0.46	0.11
SHAO	31-05-59	121-12-02	0.00	0.00	0.00	0.03

[a]DMS=degree-minute-second.

holds true as long as the polygons are properly chosen, not only in terms of area, but also of expected tectonic behavior. The constant space gradients assumption is just a first-order approximation of the underlying tectonic setting. Savage et al. (2001) give the formulation for estimating strain and rotation rates in a spherical coordinate system. The spherical solution gives insignificantly different results compared to the Cartesian approximation for networks, such as a triangulation, which is several hundred kilometers in extension.

Since the continuousness of velocity field $\mathbf{V_r}$ is unknown, but only the discrete values at points i are known, we have to use an interpolation method to obtain the velocity field $\mathbf{V_r}$ at any other point. There are many interpolation methods such as (Dermanis and Livieratos 1983): (1) finite element method (FEM)-linear interpolation within each triangle (Grafarend 1986, Straub 1996); (2) interpolation using basis functions (e.g., Haines and Holt 1993); and (3) collocation (minimum norm interpolation with infinite basis functions) (e.g., Straub and Kahle 1997). Here we will apply the FEM to do the linear interpolation within each triangle, which is optimally generated by the *Delaunay-triangulation method* among our 17 selected stations. The characteristics of Delaunay triangulation are that: (1) no triangle side is cut by another; and (2) no points are contained in any other triangle's circumscribed circle. The Delaunay triangulation of the 17 GPS sites in Shanghai is plotted in Fig. 1.

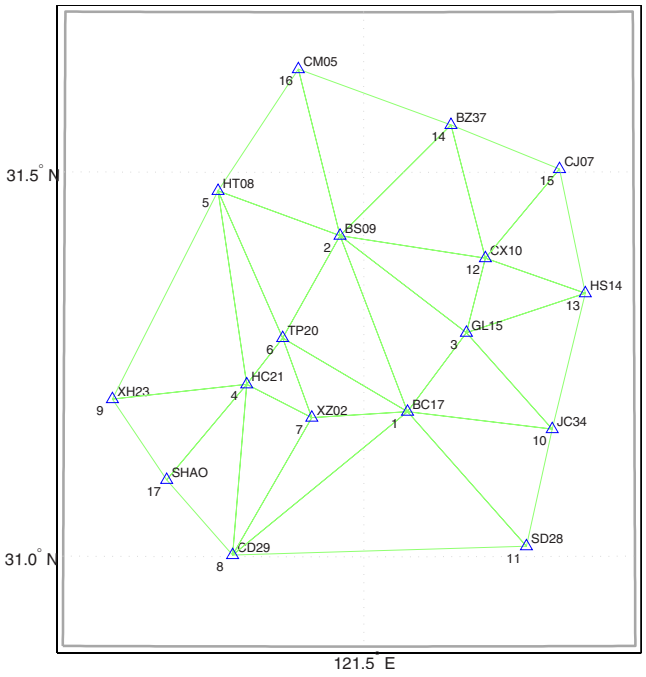

Fig. 1. Delaunay triangulation of 17 GPS sites

In FEM interpolation, for each triangle we select the centroid as the reference point, from which it is very easy to compute the velocity gradient tensor at the centroid in a very straightforward way: in fact, when dealing with three velocity vectors, the problem is solved by inverting a system of linear equations with six unknowns (four tensor components plus two velocity components of the centroid)

$$\begin{bmatrix} V_{E_1} \\ V_{N_1} \\ V_{E_2} \\ V_{N_2} \\ V_{E_3} \\ V_{N_3} \end{bmatrix} = \begin{bmatrix} 1 & 0 & \Delta E_1 & \Delta N_1 & 0 & 0 \\ 0 & 1 & 0 & 0 & \Delta E_1 & \Delta N_1 \\ 1 & 0 & \Delta E_2 & \Delta N_2 & 0 & 0 \\ 0 & 1 & 0 & 0 & \Delta E_2 & \Delta N_2 \\ 1 & 0 & \Delta E_3 & \Delta N_3 & 0 & 0 \\ 0 & 1 & 0 & 0 & \Delta E_3 & \Delta N_3 \end{bmatrix} \begin{bmatrix} V_{E_B} \\ V_{N_B} \\ \frac{\partial V_E}{\partial E} \\ \frac{\partial V_E}{\partial N} \\ \frac{\partial V_N}{\partial E} \\ \frac{\partial V_N}{\partial N} \end{bmatrix} \tag{4}$$

This approach was first proposed by Terada and Miyabe (1929). With the velocity gradient tensor we can derive the two-dimensional symmetric strain rate tensor $\mathbf{T}$ and the antisymmetric rotation rate tensor $\mathbf{R}$ at the centroid of the individual Delaunay triangle

Table 3. Strain Rate Tensor Components, Eigenspace Components, Maximum Shear Strain Rates, and Second Invariant

Triangle		Strain rate tensor components (μstrain/year) t_{11}	t_{12}	t_{22}	Eigenspace components (μstrain/year) (deg) ε_1	ε_2	α_1	Max. shear strain rate (μstrain/year) $\varepsilon_1-\varepsilon_2$	Second invariant (μstrain/year) $\sqrt{\varepsilon_1^2+\varepsilon_2^2}$
No. 1	4-5-9	−0.3097	0.1077	0.1464	0.1705	−0.3338	77.3603	0.5043	0.3748
No. 2	4-5-6	0.7384	0.0061	0.0920	0.7384	0.0919	0.5395	0.6465	0.7441
No. 3	11-1-8	0.1106	0.2399	−0.0287	0.2907	−0.2088	36.9041	0.4995	0.3579
No. 4	2-5-16	0.0799	−0.1037	0.0388	0.1651	−0.0463	−39.3993	0.2114	0.1715
No. 5	2-5-6	0.0459	−0.1395	0.0991	0.2145	−0.0695	−50.3959	0.2840	0.2255
No. 6	2-1-6	0.2459	−0.1100	0.0030	0.2883	−0.0394	−21.0798	0.3277	0.2910
No. 7	17-4-9	−0.2674	−0.0793	0.0826	0.0997	−0.2846	−77.8073	0.3843	0.3016
No. 8	17-4-8	−0.7983	0.2212	−0.0481	0.0123	−0.8586	74.7342	0.8709	0.8587
No. 9	7-4-6	0.8569	−0.0625	0.1266	0.8622	0.1213	−4.8533	0.7409	0.8707
No. 10	7-1-6	0.3213	0.0327	0.2702	0.3372	0.2543	25.9888	0.0829	0.4223
No. 11	7-4-8	0.7908	−0.1589	0.0035	0.8217	−0.0274	−10.9902	0.8491	0.8222
No. 12	7-1-8	0.3002	0.2247	−0.2764	0.3774	−0.3536	18.9667	0.7310	0.5172
No. 13	10-11-1	−0.2809	0.1056	0.0402	0.0718	−0.3125	73.3330	0.3843	0.3206
No. 14	14-2-16	0.0529	−0.0911	0.0471	0.1412	−0.0412	−44.0956	0.1824	0.1471
No. 15	3-2-1	−0.2724	−0.2201	−0.0052	0.1187	−0.3963	−60.6279	0.5150	0.4137
No. 16	3-10-13	0.0574	0.0108	−0.0809	0.0582	−0.0818	4.4371	0.1400	0.1004
No. 17	3-10-1	−0.3424	−0.1562	−0.0614	0.0082	−0.4120	−65.9846	0.4202	0.4121
No. 18	12-14-2	0.0605	−0.0235	−0.0970	0.0640	−0.1004	−8.3223	0.1644	0.1191
No. 19	12-3-2	0.0693	0.0139	0.0229	0.0731	0.0191	15.4541	0.0540	0.0756
No. 20	12-14-15	−0.0776	0.0414	−0.0545	−0.0230	−0.1091	52.7607	0.0861	0.1115
No. 21	12-15-13	−0.0114	−0.0547	0.0603	0.0898	−0.0409	−61.6355	0.1307	0.0987
No. 22	12-3-13	0.0429	0.0158	0.0237	0.0518	0.0148	29.3573	0.0370	0.0539

$$\mathbf{T} = \frac{1}{2}(\mathbf{L} + \mathbf{L}') = \begin{bmatrix} \dfrac{\partial V_E}{\partial E} & \dfrac{1}{2}\left(\dfrac{\partial V_E}{\partial N} + \dfrac{\partial V_N}{\partial E}\right) \\ \dfrac{1}{2}\left(\dfrac{\partial V_N}{\partial E} + \dfrac{\partial V_E}{\partial N}\right) & \dfrac{\partial V_N}{\partial N} \end{bmatrix} \quad (5)$$

$$\mathbf{R} = \frac{1}{2}(\mathbf{L} - \mathbf{L}') = \begin{bmatrix} 0 & \dfrac{1}{2}\left(\dfrac{\partial V_E}{\partial N} - \dfrac{\partial V_N}{\partial E}\right) \\ \dfrac{1}{2}\left(\dfrac{\partial V_N}{\partial E} - \dfrac{\partial V_E}{\partial N}\right) & 0 \end{bmatrix} \quad (6)$$

With Eqs. (4)–(6) we could compute the geodetic strain rates of 22 Delaunay triangles and successively the principal components (eigenvalues and eigendirection) together with the maximum shear strain rate $\varepsilon_1-\varepsilon_2$ and the second strain rate invariant $(\varepsilon_1^2+\varepsilon_2^2)^{1/2}$. With reference to the continued discussion in the following section, we have listed the results for these triangles in Table 3.

Representation of Numerical Results of 2D Geodetic Strain Rate and Its Interpretation

Now we can present the horizontal relative velocities and the principal strain rates of every triangle. The interpretation of them and a comparison with the geodynamical setting will follow.

The residual velocities and principal strain rates have to be represented in an appropriate way for any further interpretations and comparisons. We used the MATLAB *Mapping Toolbox* (MathWorks 2000) to map the surface deformation information. The *equidistant conic projection* was described by the Alexandrian astronomer, mathematician, and geographer Claudius Ptolemy about A.D. 150. Improvements were developed by Johannes Ruysch in 1508, Gerardus Mercator in the late 16th century, and Nicolas de l'Isle in 1745. It is also known as the simple conic or conic projection. The scale is true along all meridians and the standard parallels. It is constant along any parallel. This projection is free of distortion along the two standard parallels. Distortion is constant along any other parallel. This projection provides a compromise in distortion between conformal and equal-area conic projections, of which it is neither.

The pattern of the principal strain rates (eigenvalues and eigendirections of the 2D strain rate tensors) of 22 Delaunay triangles as well as the associated relative velocities of the 17 GPS sites in Shanghai are illustrated in Fig. 2. *Extension* is represented by symmetric arrows pointing outwards and *contraction* is represented by symmetric arrows pointing inwards. The incremental velocities are represented by *single* arrows.

In order to present the statistical information of the principal strain rates distinctly, we computed the strain rate from the residual velocities together with the 2σ formal error of their eigenspace components which is derived by the propagation of the variances of the residual velocities provided by the integrated adjustment of the multicampaigns GPS observations (Soler and van Gelder 1991, 2006; Cai and Grafarend 2007a,b). Fig. 3 shows us the pattern of the principal strain rates with 2σ formal errors of each triangle.

With these representations, we can first analyze the horizontal movements of these selected sites with respect to the SHAO station. Most of the sites show northwest-trending relative velocities with a level smaller than 1 cm/year. One exception is the GPS site BC17 whose relative velocity shows a north-east trend with a value of 0.49 cm/year. These significant relative velocities reflect the movements of these sites with respect to the base station SHAO. Second, let us analyze the principal strain rate solutions

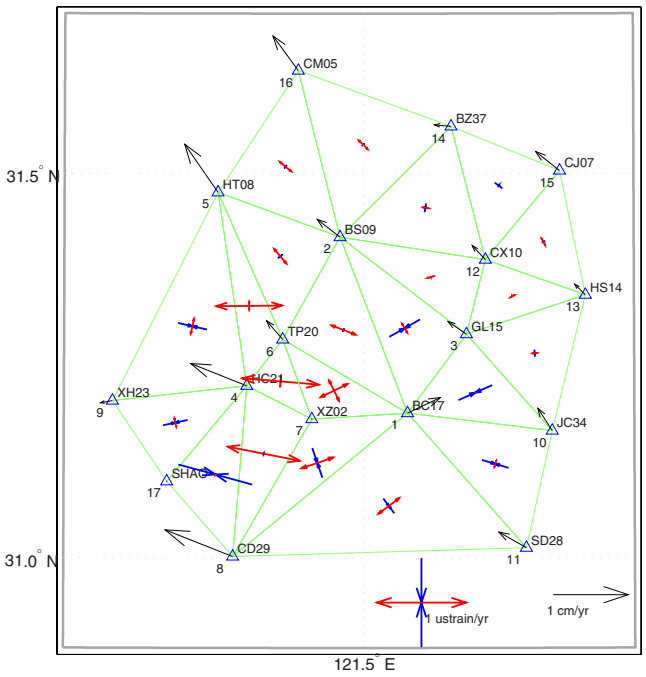

Fig. 2. Pattern of principal strain rates of each triangle and associated relative velocities of 17 GPS sites in Shanghai

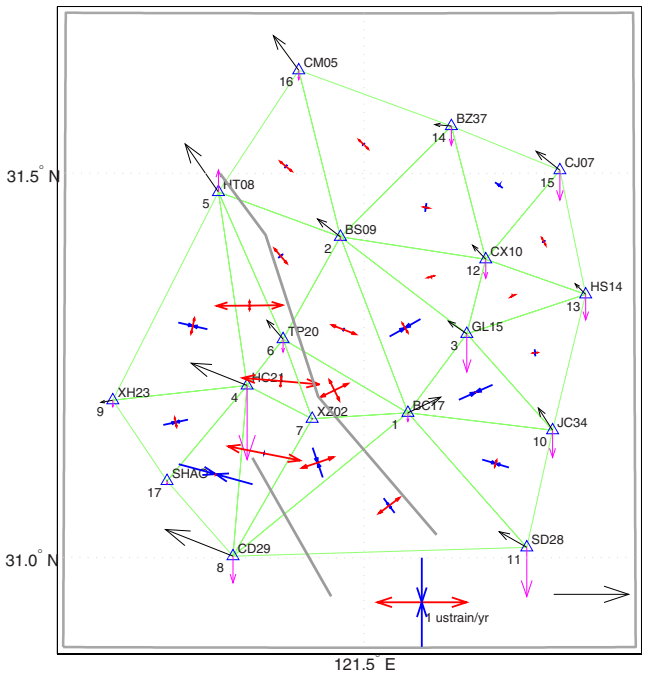

Fig. 4. Relative velocities, pattern of principal strain rates, and faults in Shanghai

of the 22 Delaunay triangles. From the derived strain rates from Eq. (5) and the visual patterns in Fig. 2, we can see that the magnitude of the principal strain rates is smaller than 1 μstrain/year. There are three distinct areas, i.e., an east, middle/southwest, and a west zone, which represent the compression, extension, and compression, respectively, whereas the strain rate field in the middle/southwestern area of Shanghai is dominated by the extension with an order of 0.8 μstrain/year. This shows that the deformation pattern of this region is characterized by a complex distribution of compressional and tensional events.

From geological and geodynamic views, the above obtained crustal deformation should reflect the neotectonic movements. Shanghai is located in the Quaternary sediment plain. The Quaternary sediment layer is between 300 and 500 m. According to Huo et al. 2004, by interpreting remote sensing images, artificial seismic explorations, and drillings, a geological fault has been identified. This so-called "Dachang–Zhoupu" fault separates the Shanghai area into two parts with a difference in the sediment complex. The Dachang–Zhoupu fault strikes N40°W and crosses the southwest of Shanghai City (Fig. 4). According to geological investigations, the fault formed in the latter part of Yanshan tectonic activity and had a significant movement during the Quaternary period (Huo et al. 2004). The fault's location agrees well with the patterns of the principal strain rates with the significant east-west extension in this area, so we can conclude that the fault may still remain active.

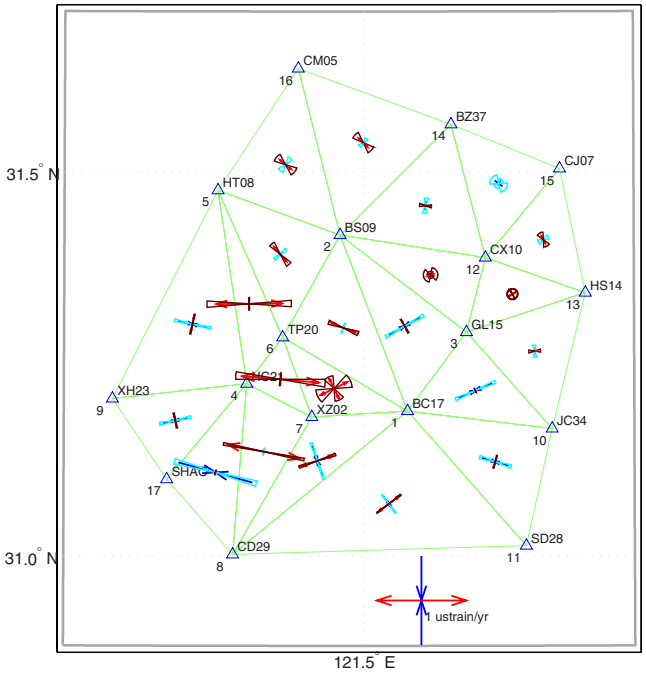

Fig. 3. Pattern of principal strain rates with 2σ formal errors of each triangle and associated relative velocities

Conclusions

With the multicampaigns GPS observations (five campaigns spanning from 2002 to 2005) of 17 GPS sites in Shanghai, the velocities of the monuments have been obtained, which are applied to estimate the strain rate tensors under infinitesimal strain assumption in each discrete Delaunay triangle. Through analysis of the horizontal movements of these sites with respect to the SHAO stations, it can be seen that most of the sites have north-west-trending relative velocities with a level smaller than 1 cm/year. Based on these relative velocities, the geodetic strain rate tensors together with their principal components of 22 Delaunay triangles are derived. Analysis of the patterns of principal strain rates shows that there are three distinct areas, i.e., an east, middle/southwest, and a west zone, which represent the compression, extension, and compression, respectively, whereas the strain rate

field in the middle/southwest area of Shanghai is dominated by the extension with an order of 0.8 μstrain/year. The ongoing crustal deformation with an extension in the middle/southwestern area of Shanghai obtained in this study is consistent with the geological settings, such as the Dachang–Zhoupu fault. In other words, our results strongly support the existence of the Dachang–Zhoupu fault. Thus, modern GPS technology supplies a useful method to detect a latency fault in city areas. For further studies we should; (1) use more continuous GPS observation stations with a better distribution in Shanghai to perform strain-rate tensor analysis; and (2) compare the geodetic strain-rate field with the geodynamic features in more detail in this area.

Acknowledgments

This work is the result of the Project Based Personal Exchange Program, PPP-China Grant No. (DAAD- D/05/26060), which is supported by the German Academic Exchange Service (DAAD) and China Education Ministry. Three anonymous reviewers provided us with constructive comments and detailed remarks in the first version of this paper. All this support is gratefully acknowledged.

References

Cai, J. (2004). "Statistical inference of the eigenspace components of a symmetric random deformation tensor." Dissertation, Deutsche Geodätische Kommission (DGK), München, Germany.

Cai, J., and Grafarend, E. (2007a). "Statistical analysis of the eigenspace components of the two-dimensional, symmetric rank-two strain rate tensor derived from the space geodetic measurements (ITRF92-ITRF2000 data sets) in central Mediterranean and Western Europe." *Geophys. J. Int.*, 168, 449–472.

Cai, J., and Grafarend, E. (2007b). "The statistical analysis of geodetic deformation (velocity and strain rate) derived from the space geodetic measurements of BIFROST project in Fennoscandia." *J. Geodyn.*, 43(2), 214–238.

Cai, J., Grafarend, E., and Schaffrin, B. (2005). "Statistical inference of the eigenspace components of a two-dimensional, symmetric rank two random tensor." *J. Geodesy, Berlin*, 78, 426–437.

Cai, J., Koivula, H., Grafarend, E., and Poutanen, M. (2008). "The statistical analysis of the eigenspace components of the strain rate tensor derived from FinnRef GPS measurements (1997-2004)." *IAG Symp. 132., VI Hotine-Marussi Symp. of Theoretical and Computational Geodesy*, Wuhan, China, P. Xu, and A. Dermanis, eds., Springer, Berlin, 79–87.

Dermanis, A., and Livieratos, E. (1983). "Application of deformation analysis in geodesy and geodynamics." *Rev. Geophys. Space Phys.*, 21(1), 41–50.

Devoti, R., et al. (2002). "Geophysical interpretations of geodetic deformations in the central Mediterranean area." *Plate boundary zones*, S. Stein and J. T. Freymuller, eds., Geodynamics Series, Vol. 30, AGU, Washington, D.C., 57–66.

Grafarend, E. (1986). "Three dimensional deformation analysis: Global vector spherical harmonic and local element representation." *Tectonophysics*, 130, 337–359.

Haines, A. J., and Holt, W. E. (1993). "A procedure for obtaining the complete horizontal motions within zones of distributed deformation from the inversion of strain rate data." *J. Geophys. Res.*, 98, 12057–12082.

Huo, E. J., Liu, C. S., Zhang, Z. Q., Yao, B. H., and Wang, F. (2004). *Shanghai latency faults and their activity*, Seismology Press, Beijing, China (in Chinese).

Kaniuth, K., and Vetter, S. (2005). "Vertical velocities of European coastal sites derived from continuous GPS observations." *GPS Solutions*, 9, 32–40.

Kim, D., Langley, R. B., Bond, J., and Shrzanowski, A. (2003). "Local deformation monitoring using GPS in an open pit mine: Initial study." *GPS Solutions*, 7, 176–185.

King, R. W., and Bock, Y. (2005). *Documentation for the GAMIT GPS analysis software version 10.20*, Massachusetts Institute of Technology, Cambridge, Mass.

Leick, A. (2004). *GPS satellite surveying*, 3rd Ed., Wiley, Hoboken, N.J.

Malvern, L. E. (1969). *Introduction to the mechanics of a continuous medium*, Prentice-Hall, Englewood Cliffs, N.J.

MathWorks (2000). *Mapping toolbox*, Version 1.2, MATLAB V 6.5, Natick, Mass.

Sagiya, T., Miyazaki, S., and Tada, T. (2000). "Continuous GPS array and present-day crustal deformation of Japan." *Pure Appl. Geophys.*, 157, 2303–2322.

Savage, J. C., Gan, W., and Svarc, J. L. (2001). "Strain accumulation and rotation in the Eastern California shear zone." *J. Geophys. Res.*, 106, 21995–22007.

Shen, Z. K., Zhao, C. K., Yin, A., Li, Y. X., Jackson, D. D., Fang, P., and Dong, D. N. (2000). "Contemporary crustal deformation in east Asia constrained by global positioning system measurements." *J. Geophys. Res.*, 105, 5721–5734.

Soler, T. (2001). "Densifying 3D GPS networks by accurate transformation of vector components." *GPS Solutions*, 4, 27–33.

Soler, T., and van Gelder, B. (1991). "On covariances of eigenvalues and eigenvectors of second rank symmetric tensors." *Geophys. J. Int.*, 105, 537–546.

Soler, T., and van Gelder, B. (2006). "Corrigendum." *Geophys. J. Int.*, 165, 382.

Straub, C. (1996). "Recent crustal deformation and strain accumulation in the Marmara SeaRegion, N. W. Anatolia, inferred from GPS Measurements." *Mitteilungen 58*, Institut für Geodäsie und Photogrammetrie, Zürich, Switzerland.

Straub, C., and Kahle, H.-G. (1997). "GPS and geologic estimates of the tectonic activity in the Marmara Sea region, NW Anatolia." *J. Geophys. Res.*, 102, 27587–27601.

Terada, T., and Miyabe, N. (1929). "Deformation of earth crust in Kiransai District and its relation to the orographic feature." *Bull. Earthquake Res. Inst., Univ. Tokyo*, 7, 223–241.

Wang, Q., et al. (2001). "Present-day crustal deformation in China constrained by global positioning system measurements." *Science*, 294, 574–577.

Wu, J. C., Tang, H. W., Chen, Y. Q., and Li, Y. X. (2006). "The current strain distribution in the North China Basin of eastern China by least-squares collocation." *J. Geodyn.*, 41, 462–470.